In-situ Raman monitoring of the poly(vinylidene fluoride) crystalline structure during a melt-spinning process

David Chapron, François Rault, Anaëlle Talbourdet, Guillaume Lemort, Cédric Cochrane, P. Bourson, Eric Devaux, Christine Campagne

In-situ Raman monitoring of the PVDF crystalline structure during a melt-spinning process

David Chapron [1], François Rault [2], Anaëlle Talbourdet [2],Guillaume Lemort [2], Cédric Cochrane [2], Patrice Bourson [1], Eric Devaux [2], and Christine Campagne [2]

[1] Université de Lorraine, CentraleSupélec, LMOPS, F-57070 Metz, France
[2] ENSAIT, GEMTEX, F-59100 Roubaix, France

Correspondence
David Chapron, Université de Lorraine, LMOPS, F-57070 Metz, France
david.chapron@univ-lorraine.fr

Funding information
Financial support from BPI France to Autonotex Project

Abstract: Poly(vinylidene fluoride) (PVDF) fibers used to develop sensors or energy harvesters have great potential in the sector of portable electronic devices and especially in the development of smart textiles. This polymorphic polymer is known for several years for its excellent piezoelectric properties related to its different crystalline phases and more particularly to the polar β-phase is the subject of studies dedicated to the development, optimization, and characterization of β-PVDF fibers. The presence and the evolution of the different crystalline phases are linked to different factors and can be controlled for example by changing some parameters during the process. In the case of the spinning process, the influence of the operating conditions, such as temperature and drawing on the crystalline structure is currently determined by post-mortem analyses. Development of "mimetic" tests to characterize in situ the evolution of the crystalline structure of a mechanically stretched polymer is a possible way. Nevertheless, this cannot totally reproduce a real process. For the first time, phase transformations and evolutions of PVDF during a melt-spinning process were studied online thanks to in-situ Raman spectroscopy measurements. Performed at different stages of the spinning line, this method allows us to follow the evolution of the crystalline phases in real-time, during the key steps of the process and to conclude on the conditions for obtaining the piezoelectric phase. The successful online characterization of PVDF crystalline phases by Raman spectroscopy opens new perspectives for the optimization of these fibers by controlling the evolution of the structure when changing process parameters.

Keywords: Melt-spinning; fibers; PVDF; β-phase; online measurements

---

1 INTRODUCTION

Since 1969 and the discovery of the piezoelectricity of PVDF by Kawai [1] many researchers have studied the different methods for improving the piezoelectric character of this polymer. It is well known that PVDF shows five crystalline polymorphs (α, ε, γ, δ, and β). The two first ones are non-polar due to the antiparallel packing of the dipoles whereas the other three crystalline structures are polar and show piezoelectric character. Among them, the last one (β-phase) is the most interesting from this point of view. The α-phase is predominantly obtained during crystallization from the melt during common cooling conditions. Indeed, during an initial cooling, the polymer crystallizes spontaneously in its α-phase. Several articles report studies on the optimization of the β-phase with piezoelectric

properties by: addition of nano-sized fillers [2], annealing [3–5], or uni-axial drawing. Mechanical stress is one of the most important factors to obtain the β-phase of PVDF. The transformation of the non-polar α-phase into the β-phase requires a certain draw ratio and temperature. This mechanism of α→β transformation during drawing has been discussed by several authors [6–10]. Initial studies were conducted on PVDF films. Sajkiewicz [11] concluded the draw ratios must be between 1 and 7 with a temperature range between 50 and 145°C for obtaining the β-phase. A large number of authors have focused on optimization of this polar phase [9], like Salimi [7] who exhibits a PVDF film optimized at 74% β-phase by a ratio between 4.5 and 5 at 90°C. Mohammadi [12] optimizes a film with 86.5% β-phase with a draw ratio of 6.5 at 87°C. According to these first studies, the evolution of the crystalline phases has also been studied after the particular spinning process resulting in the production of filaments [13]. By studies made after the end of filament production, Lund et al. [14] demonstrate that obtaining 80% β-phase in PVDF is caused by the draw ratio imposed by the speed of the rolls and the temperatures of process. All these studies were carried out post-spinning (ex-situ). In the case of the melt-spinning process, the studies highlight the need for the uniaxial drawing step for optimizing the piezoelectric β-phase content of PVDF. The studies of crystalline phases after the melt spinning process are carried out by using several characterization techniques: infrared spectroscopy [15,16], X-ray diffraction (XRD) [13,17] also wide-angle and small-angle X-ray scattering (WAXS and SAXS) [13,18,19]. Nevertheless, all these studies are carried out the post-spinning process and give the final state of the PVDF crystalline phases without following the evolution of polymer structure along this process. Raman spectroscopy is an adapted optical probe to study the morphology of semi-crystalline polymer phases during the phase transition process [20]. Raman spectra of PVDF are already well known especially for α, β and amorphous phases [21,22,25,26]. The phase transition α to β can occur under temperature by application of a mechanical strain (under shear, by stretching, by spinning) and Raman spectroscopy could be used *in situ* on a process, for example during the stretching of PVDF films [23].

Here we present the study of the evolution of the crystalline phases, mainly the α-phase and β-phase, directly on a melt-spinning pilot using Raman spectroscopy. This method makes it possible to understand which stage of the spinning process leads to the transformation of the phases. The laser used during Raman experiments has therefore been placed at six strategic locations on the spinning line, making it possible to study the crystalline structure of the PVDF at the exit of the spinnerets, during drawing and before winding.

2 MATERIALS AND METHODS

Polymer - Commercial spinning PVDF homopolymer grade, Kynar®705 supplied by Arkema (France) in pellet form was used. The following characteristics were given by the supplier: the melt flow index (MFI) is 25 g.10min^{-1} under a load of 2.16 kg at 220°C, the melting temperature T_m is 173 °C and the density is 1.76 g.cm^{-3}.

Melt-Spinning of the multifilaments - The PVDF multifilaments are produced on a melt-spinning pilot, Spinboy I, manufactured by Busschaert Engineering (Outrijve, Belgium), whose principle is shown schematically in Figure 1. Before melt-spinning, the PVDF pellets are dried in an oven for several hours to eliminate moisture and thus facilitate the spinning process. The pellets are subsequently introduced into the feed hopper from the top of the spinning line. A single-screw extruder melts and conveys under pressure the polymer to the spinnerets. The extrusion is done according to a temperature profile set between 195°C and 225°C. The polymer is then conveyed to the spinnerets using a volumetric pump. This first part that reaches the molten polymer output extruder ensures a

constant flow of material, according to a rotational speed of 20 rpm with the polymer material. The passage through the spinnerets makes it possible to shape the filaments according to the desired profile. The spinneret used had two parts with 40 holes with a diameter of 1.2 mm for each one. After the spinnerets, the multifilaments are rapidly cooled by thermal quenching using fresh air at room temperature propelled in the direction transverse to the production to solidify the polymer. After cooling by fresh air, the multifilaments then pass into a sizing gutter. The sizing is a mixture of oil and water. This step lubricates the filaments and thus facilitates the sliding of the latter on the different metal parts of the pilot, also eliminate the electrostatic effect of friction and finally give cohesion between the filaments. The PVDF multifilaments are recovered on the roll (R_0), the alimentation roll (R_1), and the drawing roll (R_2) heated respectively at 70°C, 110 °C and 90 °C. Between roll R_1 and R_2, the multifilament was drawn by adjusting the speed of the rolls. The multifilaments are wound on 7 turns around the roll R_1, 3 turns on the roll R_2. These turns can retransmit the movement, the speed of the rolls to impose the right drawing indicated. No drawing takes place between R_0 and R_1 because the multifilaments slide on the roll R_0 which serves exclusively to direct the multifilaments. The final crystal morphology is highly dependent on the spinning parameters used. The speed of R_2 has been stabilized at 500 m.min^{-1} to obtain multifilaments of the same linear mass. The velocity ratio R_2/R_1 represents the theoretical draw ratio (λ). In the following tests, this one was carried out at 1.25 and 4. Finally, the multifilament of 246 tex (g.1000m^{-1}) was recovered on a final bobbin.

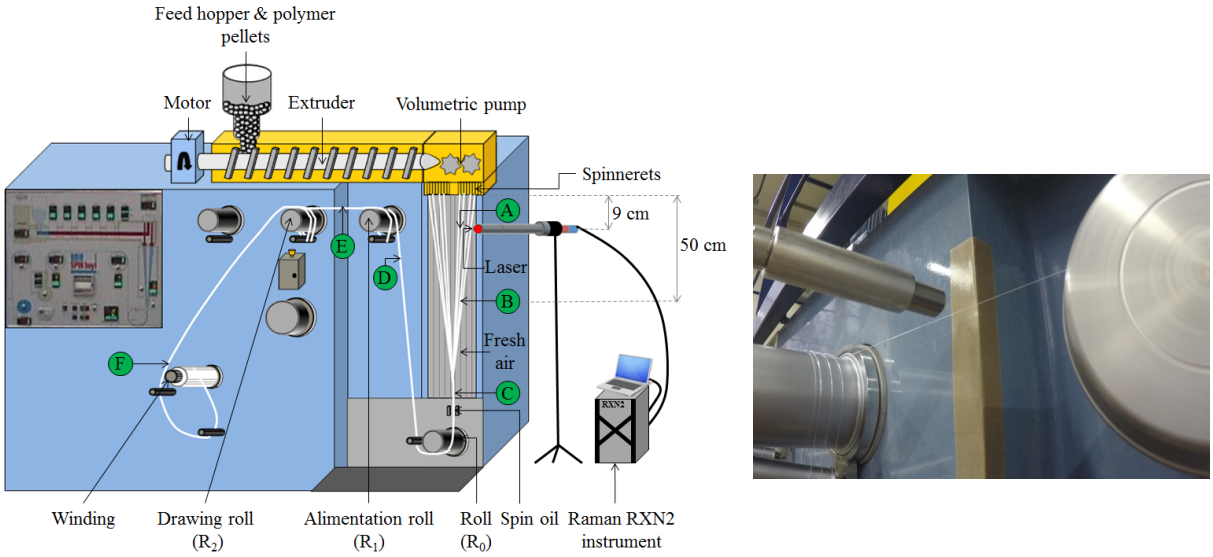

Figure 1. Pilot of multifilaments melt-spinning process and different positions of the laser (A-F). Picture of a measurement with the Raman probe on the multifilament.

In situ Raman Spectroscopy Measurements – Raman scattering experiments were performed *in situ*, directly on the melt-spinning pilot with a RXN2 Raman spectrometer from Kaiser Optical Systems. The power of the 785 nm laser was 400 mW and the Raman probe focal distance was 2 cm (Figure 1). The laser beam on the sample was unpolarized as multimode fibers were used for the excitation and collection paths. All Raman spectra were recorded between 100 cm^{-1} and 3500 cm^{-1} with a spectral resolution around 4 cm^{-1}. The integration time was 45 s and each spectrum was recorded 3 times and averaged. The Raman laser was moved along the melt-spinning line to measure the crystalline phases at different locations. Despite lateral vibrations of fibres, with a multifilament diameter around 4mm (80 filaments of 50µm each) and estimated laser spot diameter and focal depth

of 20µm and 100µm respectively, during the integration time all the multifilament fibre stay in the probed volume. Three positions are located between the extruder and the roller R_0: 9 cm from the spinneret (position A), 50 cm from the spinneret (position B), and finally just before the sizing gutter (position C). The last three positions are between the roll R_0 and the winding: just before R_1 (position D), between R_1 and R_2 (position E) show in Figure 2, and finally before the winding (position F). The fractions of the crystalline phases are measured from the surface area measurement under the representative peaks of the phases. The presence of the amorphous phase must therefore be taken into account in each result.

Micro-Raman Spectroscopy Measurement – Ex situ Raman measurements on PVDF samples were performed with a micro-Raman spectrometer LabRAM HR from Horiba Jobin with a 785 nm laser line at 200 mW with a 100x microscope objective. The spectral resolution was 1 cm^{-1}.

3 RESULTS AND DISCUSSION

The evolution of the crystalline phases is studied in real-time at the different key steps of the melt-spinning process. The phase change within the PVDF is particularly due to the conditions of the process, such as temperature and drawing. To observe the phase transformations, the different Raman spectra were collected for two different theoretical draw ratios (λ) of 1.25 and 4. The second theoretical draw ratio (λ=4) was chosen because an α→β transformation is expected due to the stress met during all the spinning process whereas a low theoretical draw ratio was fixed to confirm a previous hypothesis, *i.e.*: a sufficient high uniaxial stress is needed to lead to the crystalline structure modification.

Figure 2 shows the Raman spectra of two PVDF samples with draw ratios of 1.25 and 4. The difference between the spectra is mainly due to the crystalline phases: mostly in β-phase at high λ and in α-phase at low λ. The assignment of the vibrational bands of α and β phases of PVDF were reported in [24] [25]. As the more intense peaks of the crystalline phases are between 750 and 900 cm^{-1} [26][27], the study and the following fitting procedures will be focused on this spectral domain. The characteristic wavenumbers of the different phases of the PVDF are: the peak at 839 cm^{-1} for the β-phase and the 795 and 874 cm^{-1} peaks for the α-phase. The complexity of the on-line measurements due to the movements of the multifilaments on the spinning pilot brings disparity of the raw spectral intensities. It requires then a standardization step before comparison, therefore a linear baseline correction and a normalization process according to the area of the peaks between 750 cm^{-1} and 900 cm^{-1} is performed for each spectrum at different positions.

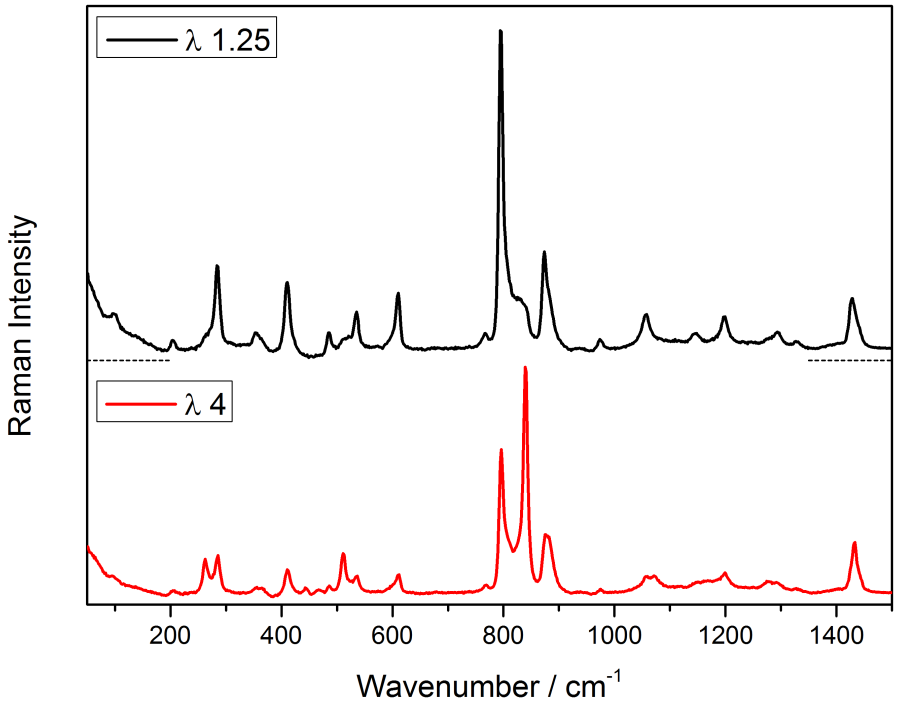

Figure 2. Raman spectra of PVDF multifilament samples at λ=1.25 (rich in α-phase) and 4 (rich in β-phase) measured with Micro-Raman spectrometer.

The experimental Raman spectrum between two boundaries includes bands and shoulders representing the crystalline and amorphous phases of the polymer. For greater accuracy in spectra analyses and to improve the understanding of phases behaviour, each *in situ* spectrum has been decomposed using a fitting procedure. In semi-crystalline polymers, the spectral signatures of amorphous and crystalline phases have a Gaussian and a Lorentzian profile respectively. As a result, the calculations of fraction crystallinity of each phase (F_{α}, F_{β}) and total crystalline and amorphous rates (F_{cryst}, F_{am}) presented in this study were calculated with the fitting parameters. All spectra were fitted with the same spectral model by fixing all band centres: two Lorentzian bands at 795 and 874 cm^{-1} for the α-phase (L_{α}), one Lorentzian band at 839 cm^{-1} for the β-phase (L_{β}) and four Gaussian bands at 797, 809, 830 and 881 cm^{-1} (G). The model is presented in Figure 3. The fractions of the crystalline phases are measured from the integration method of the representative peaks of the different phases (795 cm^{-1} and 840 cm^{-1}). The estimation of the fraction of α-phase in the total crystalline phase is calculated according to **Equation 1**.

Equation 1

$$F(\alpha) = \frac{\sum A_{\alpha\ Lorentzian}}{\sum A_{\alpha\ Lorentzian} + \sum A_{\beta\ Lorentzian}}$$

Where $A_{\alpha\ Lorentzian}$ and $A_{\beta\ Lorentzian}$ are areas calculated after integration of corresponding Lorentzian peaks

The following spectra will be presented according to their position on the melt spinning line. At first, the evolution of the crystalline phases will be studied between the dies and the roll R_0. In a second step, the phase transformations will be analysed between R_0 and the winding. As illustrated in Figure 3 and 4, the main difficulty in the fitting procedure is the estimation of the crystalline phase from the amorphous band in the case of the PVDF α-phase. Thus in the first positions A, B, C, where the crystalline peaks are weak and the Lorentzian and Gaussian peak centers are close the error on F_α are higher than on others positions.

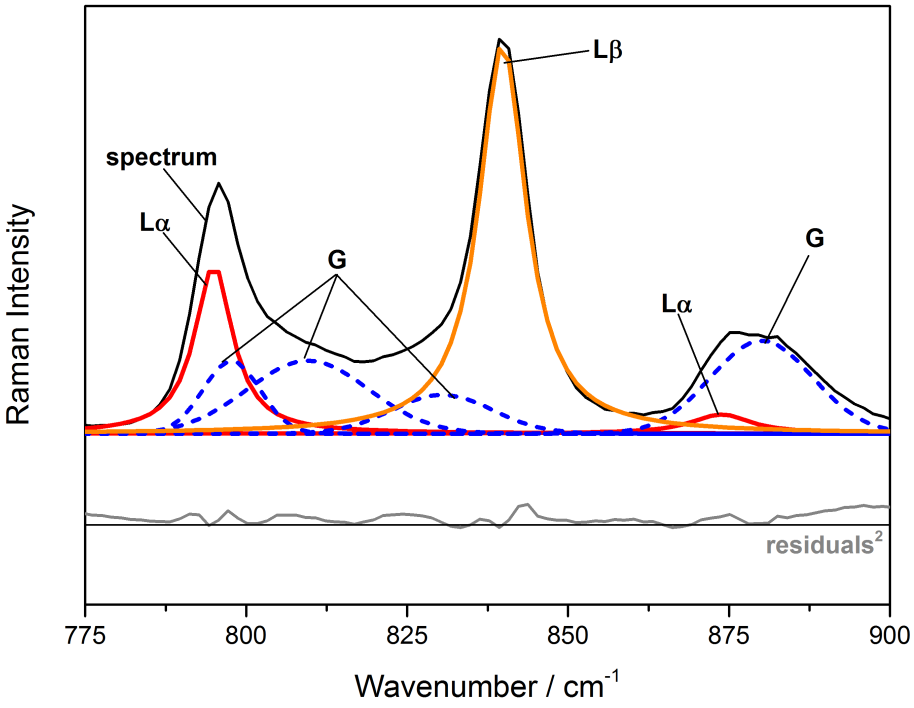

Figure 3. Example of decomposition (three Lorentzian peaks: L_α and L_β, and four Gaussian peaks: G) applied on the Raman spectrum between 750 and 900 cm^{-1} on a sample with $\lambda = 4$. The squared residuals, between the measured spectrum and the fit, are show in the bottom.

3.1. Positions between the spinneret and the roll R_0.

Figure 4 shows the Raman spectra collected at the A, B, and C positions for a theoretical draw ratio $\lambda = 4$. The α-phase intensity (795 and 874 cm^{-1}) is significant directly after the spinnerets output, the peak appears between A and B and is increasing along the B and C falling and cooling process. At the same time, around 840 cm^{-1}, the β-phase signature does not come off the amorphous shoulder. Despite the polymer falling and drawing under its weight between the dies and the roll R_0, the PVDF does not know any significant α→β transformation at these three positions.

In the very first part of the spinning process, whatever the draw ratio used polymer crystallization occurs mainly under α-phase as proven by a high intensity of the band at 795 cm^{-1}.

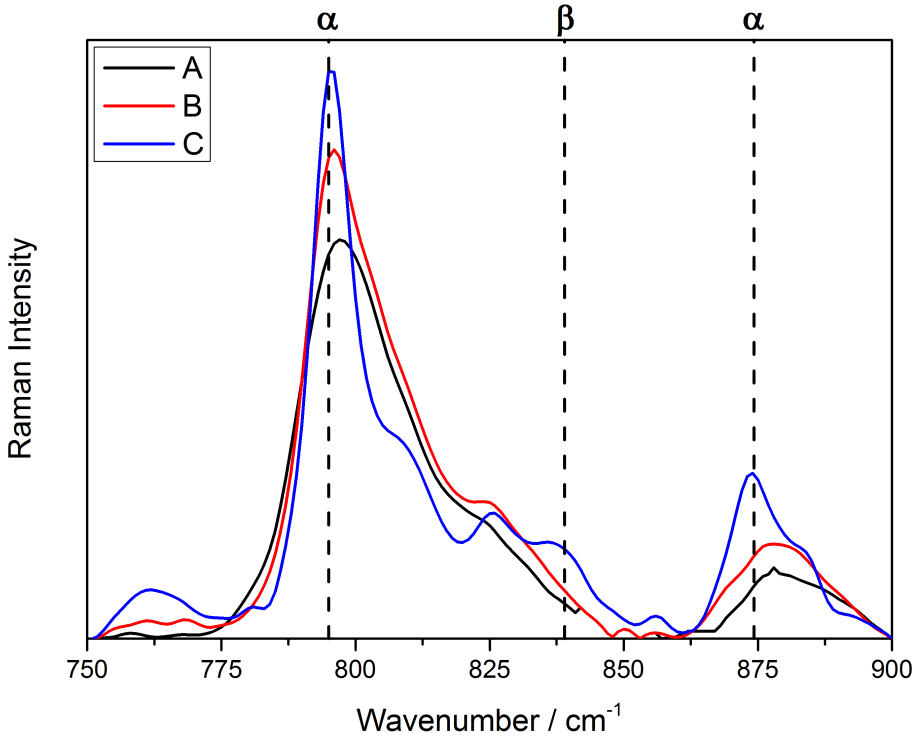

Figure 4. In situ Raman spectra at draw ratio λ = 4 and A, B and, C positions. Evolution of the intensity bands A_α and A_β.

3.2. Positions between the roll R_0 and the winder

Figure shows the Raman spectra of the D, E, and F positions for a draw ratio λ = 4.

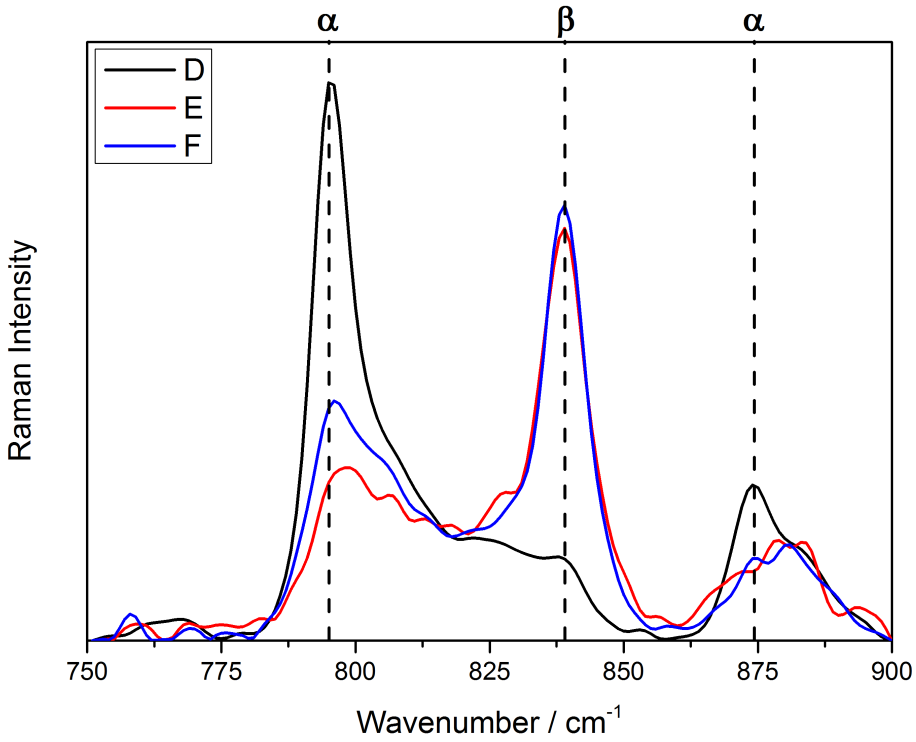

Figure 5. In situ Raman spectra at draw ratio λ = 4 and D, E and F positions. Evolution of the intensity bands A_α and A_β.

Position D is located just before roll R_1, the spectrum is similar to the spectrum in the C location, and the transition C-D doesn't influence the crystalline structure of the polymer. In E position, between R_1 and R_2, the intensity of the peak at 839 cm^{-1} sharply increasing which reveals the appearance of the β-phase. Conversely, from the drawing roller R_1, the characteristic band α decreases in intensity in favour of the β band. This observation is directly related to the conformational transformation of the macromolecular chain generated by the drawing between the rolls R_1 and R_2.

The β-phase appears exclusively from the roll R_1 and thus the uniaxial drawing imposed by the speed ratio of the rollers R_2 and R_1, as shown in Figure in position E. In position F, the characteristic peak of the β-phase is stable but that of the α-phase slightly increases compared to the position E.

The α→β phase transformation is therefore mainly caused by the uniaxial drawing imposed by the speed difference between the rollers R_1 and R_2. Indeed, at the same position E (between the two rollers), the β-phase content remains non-existent for a weak drawing of λ = 1.25 (Figure) where the main characteristic band of this spectrum represents the crystalline α-phase.

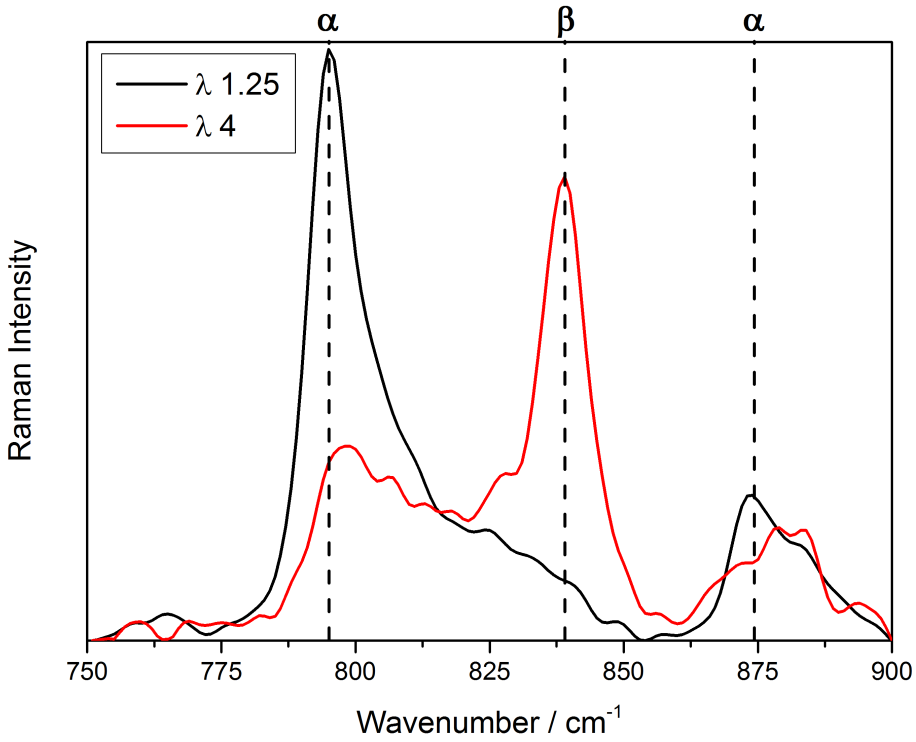

Figure 6. In situ Raman spectra at draw ratio λ = 1.25 and λ = 4 in E position. Evolution of the intensity bands A_α and A_β

Table 1 shows the fractions in α and β-phase as a function of the draw ratio and also of the position of the laser in the line, measured by the method of integration of the areas under the Lorentzian peaks after decomposition. To study the evolution of the Raman spectrum after melt-spinning, static Raman measurements were performed on samples recovered on a reel, two months after spinning the filaments

The melt-spinning process of PVDF allows controlling the crystalline phase with the draw ratio parameter. For both draw ratios 1.25 and 4, the fraction of the crystalline phase compared to the amorphous one is significant and these values are slightly constant after two months, which indicates the stability of crystalline phases of PVDF.

Thus, Raman spectroscopy is a promising technique to follow in situ the morphological development of polymer fibers. The study of the adjustments can then be optimized in order to simply use this technique as optical sensors for in situ measurement.

4 CONCLUSIONS

These measurements of *in-situ* Raman spectroscopy on a melt-spinning pilot made it possible to define the optimal conditions to obtain the β-crystalline phase. Despite the spinning speeds and the drawing has undergone by the polymer directly at the exit of the spinnerets, no evolution of the β-phase is observable before the uni-axial drawing imposed by the ratio of the speeds of the rolls R_2 and R_1. This drawing must also be important. Indeed, for a draw λ = 1.25, the β-phase content has not changed over the entire spinning

line. For the study of the β-phase of PVDF in line, it is then necessary to orientate the laser from the first roller causing drawing.

ACKNOWLEDGEMENTS

Authors are grateful for financial support from BPI France and Arkema to Autonotex Project.

ORCID

David Chapron https://orcid.org/0000-0002-0738-6626
François Rault https://orcid.org/0000-0002-0495-2047
Cédric Cochrane https://orcid.org/0000-0002-4363-1721
Patrice Bourson https://orcid.org/0000-0002-3541-3257
Eric Devaux https://orcid.org/0000-0003-0850-138X
Christine Campagne https://orcid.org/0000-0001-5223-0236

REFERENCES

[1] H. Kawai, *Jpn. J. Appl. Phys.* **1969**, *8*, 975.
[2] G. H. Kim, S. M. Hong, Y. Seo, *Phys. Chem. Chem. Phys.* **2009**, *11*, 10506.
[3] S. Satapathy, S. Pawar, P. K. Gupta, K. B. R. Varma, *Bull. Mater. Sci.* **2011**, *34*, 727.
[4] C. Marega, A. Marigo, *Eur. Polym. J.* **2003**, *39*, 1713.
[5] M. Neidhöfer, F. Beaume, L. Ibos, A. Bernès, C. Lacabanne, *Polymer (Guildf).* **2004**, *45*, 1679.
[6] P. Martins, A. C. Lopes, S. Lanceros-Mendez, *Prog. Polym. Sci.* **2014**, *39*, 683.
[7] A. Salimi, A. A. Yousefi, *Polym. Test.* **2003**, *22*, 699.
[8] R. Gregório, D. S. Borges, *Polymer (Guildf).* **2008**, *49*, 4009.
[9] J. Gomes, J. Serrado Nunes, V. Sencadas, S. Lanceros-méndez, *Smart Mater. Struct.* **2010**, *19*, 65010.
[10] V. Sencadas, M. V Moreira, S. Lanceros-Méndez, A. S. Pouzada, R. Gregório, *Mater. Sci. Forum* **2006**, *514–516*, 872.
[11] P. Sajkiewicz, A. Wasiak, Z. Gocłowski, *Eur. Polym. J.* **1999**, *35*, 423.
[12] B. Mohammadi, A. A. Yousefi, S. M. Bellah, *Polym. Test.* **2007**, *26*, 42.
[13] C. Du, B. Zhu, Y. Xu, *J. Appl. Polym. Sci.* **2007**, 104, 2254.
[14] A. Lund, B. Hagström, *J. Appl. Polym. Sci.* **2010,** 116, 2685.
[15] Z. Guo, E. Nilsson, M. Rigdahl, B. Hagström, *J. Appl. Polym. Sci.* **2013**, *130*, 2603.
[16] K. Magniez, A. Krajewski, M. Neuenhofer, R. Helmer, *J. Appl. Polym. Sci.* **2013**, *129*, 2699.
[17] A. Lund, B. Hagström, *J. Appl. Polym. Sci.* **2011**, *120*, 1080.
[18] W. Steinmann, S. Walter, G. Seide, T. Gries, G. Roth, M. Schubnell, *J. Appl. Polym. Sci.* **2011**, *120*, 21.
[19] S. Walter, W. Steinmann, J. Schütte, G. Seide, T. Gries, G. Roth, P. Wierach, M. Sinapius, *Mater. Technol. Adv. Perform. Mater.* **2011**, *26*, 140.
[20] M. Ponçot, J. Martin, S. Chaudemanche, O. Ferry, T. Schenk, J.P. Tinnes, D. Chapron, I. Royaud, A. Dahoun, P. Bourson, *Polymer* **2015**, 80, 27-37

[21] Y. Yang, G. Wu, S. Ramalingam, S.L. Hsu, L. Kleiner, F.W. Tang, *Macromolecules* **2007**, 40(26), 9658–9663

[22] M. Veitmann, D. Chapron, S. Bizet, S. Devisme, J. Guilment, I. Royaud, M. Poncot, P. Bourson, *Polymer Testing* **2015**, 48, 120-124

[23] M. T. Riosbaas, K. J. Loh, G. O'Bryan, and B. R. Loyola, Proc. *SPIE 9061, Sensors and Smart Structures Technologies for Civil, Mechanical, and Aerospace Systems* **2014**, 90610Z (10 April 2014)

[24] F.J. Boerio, J. L. Koenig, *J. Polym. Sc. Part A-2: Polymer Physics* **1971**, 9 (8), 1517–1523.

[25] M. Kobayashi, K. Tashiro, H. Tadokoro, *Macromolecules* **1975**, 8 (2), 158–171.

[26] T. Boccaccio, A. Bottino, G. Capannelli, P. Piaggio, *J. Memb. Sci.* **2002**, *210*, 315.

[27] C. J. L. Constantino, A. E. Job, R. D. Simões, J. A. Giacometti, V. Zucolotto, O. N. Oliveira, G. Gozzi, D. L. Chinaglia, *Appl. Spectrosc.* **2005**, *59*, 275.

Table 1. Evolution of α-phase and β-phase ratios in PVDF measured by Raman spectroscopy as a function of the draw ratio λ and position on the spinning line, according to Equation 1. Micro-Raman measurements were done on samples after two months.

	λ = 1.25				**λ = 4**			
	F_{am}(%)	F_{cryst} (%)	In crystal. phase		F_{am}(%)	F_{cryst} (%)	In crystal. phase	
Positions			F_{α} (%)	F_{β} (%)			F_{α} (%)	F_{β} (%)
A	100	0	-	-	100	0	-	-
B	91	9	100	0	89	11	100	0
C	67	33	100	0	64	36	98	2
D	65	35	100	0	68	32	97	3
E	63	37	100	0	42	58	30	70
F	54	46	100	0	45	55	33	67
Micro-Raman	52	48	99	1	40	60	29	71